第 49 卷 第 2 期/2022 年 1 月/中国激光 研究论文

中国激光

激光-电弧复合焊在坡口中的等离子体耦合行为

周建，邵晨东，崔海超*，唐新华，芦凤桂

上海交通大学材料科学与工程学院，上海 200240

摘要 研究了在坡口中进行复合焊时激光和电弧的耦合行为，结果表明：当光丝间距为 2 mm 时，激光和电弧能够持续耦合，但熔池表面波动剧烈，焊接飞溅较大，表面成形较差；当光丝间距为 4 mm 时，激光和电弧等离子体出现周期性耦合，熔池表面波动较小，焊缝表面成形较好。出现周期性耦合主要是因为焊丝熔化后先填充坡口，造成电弧下方液体堆积，激光作用区域和电弧作用区域的高度不在同一水平面上，使得实际光丝间距大于 4 mm，激光和电弧不耦合；当堆积液体达到一定高度后，在重力和表面张力作用下液体向激光作用区域流淌，液面趋于水平，实际光丝间距接近 4 mm，激光和电弧等离子体连接在一起，再次发生耦合。当光丝间距大于 6 mm 时，激光和电弧不发生耦合。

关键词 激光技术；激光-电弧复合焊；低合金高强钢；坡口；耦合机理

中图分类号 TG456.7 **文献标志码** A **doi**：10.3788/CJL202249.0202006

1 引 言

中厚板低合金高强钢（厚度大于 4 mm）被广泛应用于工程机械等领域，其应用主要通过焊接来实现，焊接方法主要包括多层多道气体保护焊、窄间隙埋弧焊、穿孔等离子弧焊、激光焊、激光填丝焊、激光复合焊、真空电子束焊以及摩擦焊等[1-4]。中厚板低合金高强钢的焊接难题主要集中在焊缝成形、焊缝和母材的强韧性匹配、热影响区软化以及焊后残余应力和焊接变形等方面[5-8]。针对厚度较大的低合金高强钢的焊接，譬如转子钢焊接等，工业上普遍采用多层多道窄间隙埋弧焊方法[9-10]，焊缝成形较好，焊缝及热影响区的综合性能较好。但针对结构用钢焊接，受其工作条件限制，多采用手工电弧焊焊接，工作效率较低，且焊接过程一致性较差。

关于中厚板焊接，有学者采用纯激光直接进行焊接，但焊接深度并不与激光功率成线性关系，主要是因为高功率激光深熔焊时会产生大量等离子体和金属蒸气羽烟，对激光能量有衰减作用；另外，当焊接深度增加时，焊缝表面成形较难控制，容易出现咬边等缺陷[11]。因此，很多学者采用激光复合焊方法开展中厚板焊接研究，利用激光和电弧双重热源，依靠电弧在前、激光在后的焊接工艺，提高材料对激光的吸收率，同时稳定焊接小孔，增加焊接熔深。Zhan 等[12]采用激光-MIG 复合多层多道焊的方式得到成形良好的焊接接头，实现了 19.05 mm 厚 Invar 合金的有效连接。大量学者研究了在平板上面直接进行激光复合焊，并对焊接过程中的电弧和激光耦合机理、熔滴过渡形态、焊缝成形以及焊缝性能等方面开展了大量的研究[13-18]。在激光复合焊中，为了增加熔深，上部一般会开坡口，依靠激光增加焊接深度并利用电弧进行盖面填充，既能保证焊缝深度，又能确保焊缝成形质量[19]，使得激光-电弧复合焊在中厚板焊接领域得到广泛应用，在坡口中进行激光-电弧复合焊接时，随着熔池波动，熔池内液体填充坡口，导致电弧和激光不在同一水平面内，电弧和激光耦合效果也随之改变，这一点与激光和电弧平板焊接时明显不同，但针对激光和电弧在坡口中的耦合机理研究较少。

本文针对中国宝武生产的 16 mm 厚 BG890QL

收稿日期：2021-05-06；**修回日期**：2021-06-02；**录用日期**：2021-07-08

通信作者：*haichaocui@sjtu.edu.cn

低合金高强钢中厚板，通过对中厚板表面开坡口，采用激光复合焊方法，通过高速摄像机观察坡口中激光复合焊接时的等离子体形貌及熔池流动特征，并结合焊缝成形特征，分析坡口中激光和电弧复合焊的耦合机理，为激光-电弧复合焊在厚板开坡口焊接时提供理论指导和工程应用参考。

2 试验材料及方法

本试验所采用的 BG890QL 钢是由中国宝武钢铁集团有限公司生产提供，主要元素含量如表 1 所示。BG890QL 钢经过熔炼轧制后在 640 ℃进行高温回火处理，保温 60 min 后空冷，获得的组织为回火马氏体。

表 1 BG890QL 钢的主要化学成分

Table 1 Main chemical compositions for BG890QL steel

Element	C	Si	Mn	Cr	Mo	Nb	V	Ni	W	Fe
Mass fraction /%	0.18	0.47	1.10	0.78	0.05	0.05	0.07	0.16	0.53	Bal.

激光焊接系统采用 IPG Photonics 公司生产的 10 kW 级光纤激光器(IPG-10000)，电弧焊系统采用 Fronius 生产的全数字化焊机(TPS 5000)。焊接时板材坡口如图 1 所示。本研究中激光和电弧之间的光丝间距 d 为激光光斑在坡口底部的投影与电弧焊丝延长线与坡口底部交点之间的距离，具体如图 2 所示。根据前期的工艺探索，选用激光功率为 7 kW，弧焊电流为 240 A，焊接电压为 22 V，焊接速度为 0.5 m/min 进行激光-电弧复合焊。

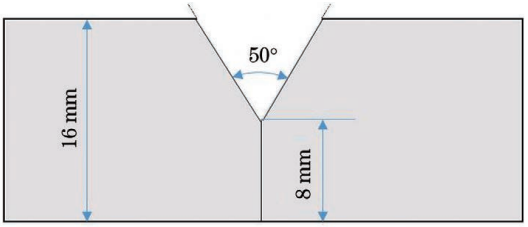

图 1 激光-电弧复合焊时坡口形状及尺寸

Fig. 1 Profile of single groove in laser-arc hybrid welding

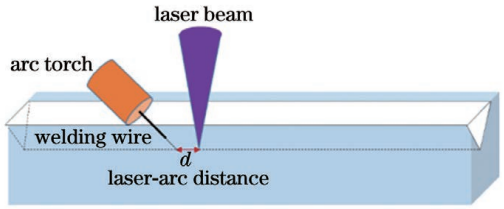

图 2 光丝间距示意图

Fig. 2 Schematic of distance between laser spot and wire tip

3 试验结果及分析

3.1 坡口中激光-电弧复合焊的等离子体行为

在激光-电弧复合焊过程中，激光和电弧的相对位置对焊缝成形有重要影响。当电弧在前、激光在后时，文献[20-21]已经指出，激光产生的等离子体稳定了电弧，同时：电弧在前，可预热熔化金属，有助于提高金属对激光的吸收率，增加熔深；激光在后，可直接照射到液态金属上，导致液态金属直接汽化，形成的飞溅较多，对焊缝表面成形不利。有鉴于此，本试验重点研究激光引导、电弧跟随时，不同光丝间距对激光和电弧耦合行为的影响。

图 3～5 分别展示了光丝间距 d 为 2，4，6 mm 时，激光和电弧在 V 型坡口中的等离子体形貌。由于拍摄等离子体时加入了滤光光源，可以拍摄到波长为 400～950 nm 的谱线，因此从所拍摄图片中不仅可以观察到该波段的等离子体形貌，还可以观察到熔池形态。当光丝间距为 2 mm 时，图 3(a)～(d)所示为起焊时等离子体形态，图 3(e)～(h)所示为焊接稳定后的等离子体形态。从图 3(a)可以看到，起焊时激光和电弧直接作用；从图 3(b)所示的等离子体耦合后形貌可以看到，等离子体完全重合，电弧和激光完全耦合，亮度较强，体积相对减小。随着热源移动，电弧和激光等离子体一直连接[图 3(d)]，且等离子体区域的面积逐渐增大。当焊接稳定后，焊丝熔化填充坡口，导致整个熔池液面上升，使得激光作用位置和电弧之间距离相较于起焊时有所增加，两者之间的等离子体微弱连接[图 3(e)]。随着热源继续移动，流体继续填充坡口，激光直接照射到坡口中的流体上面，流体表面不规则导致激光区域等离子体形状变得不规则，但激光照射区域和电弧区域的相对距离减小，激光和电弧逐步开始耦合[图 3(f)]；随后熔化金属增多，填满坡口，整个熔池液面高度趋于一致，激光和电弧完全耦合[图 3(g)]。此时整个熔池液面较高，激光和电弧等离子体耦合时，等离子体面积相较于起焊时增大，等离子体亮度减弱[图 3(h)]。

当光丝间距为 4 mm 时，起焊时激光和电弧等离子体并没有完全连接，激光和电弧等离子体没有发生耦合，如图 4(a)所示。随着热源移动，激光和电弧等离子开始连接，发生耦合[图4(b)]，但整个

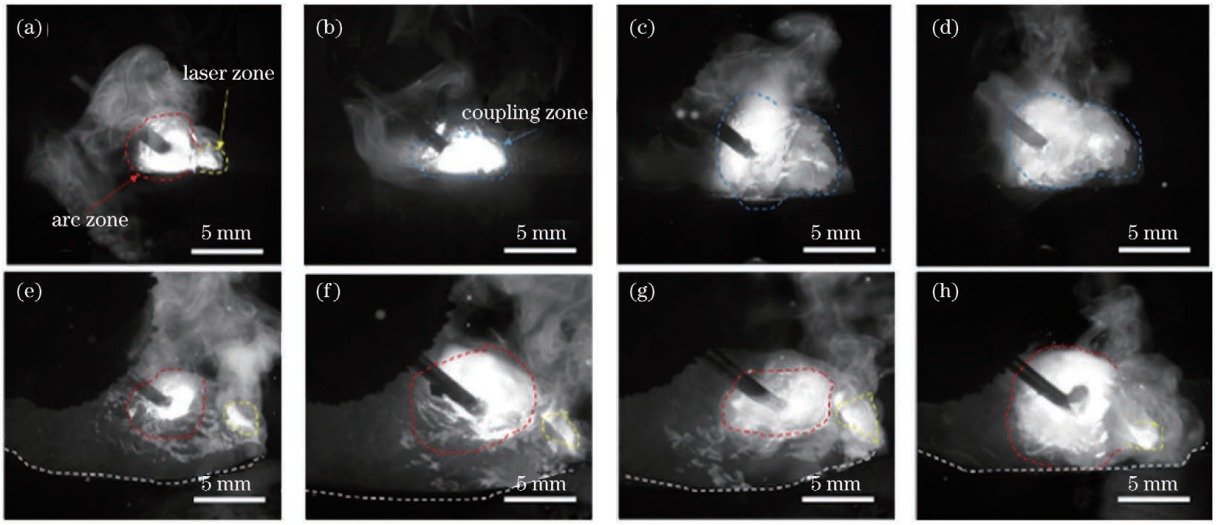

图 3 $d=2$ mm 时不同时刻激光和电弧等离子体形貌。(a)$t=0$ s;(b)$t=0.01$ s;(c)$t=0.02$ s;(d)$t=0.03$ s;(e)$t=3.01$ s;(f)$t=3.02$ s;(g)$t=3.03$ s;(h)$t=3.04$ s

Fig. 3 Profiles of laser and arc plasma at different moments with $d=2$ mm. (a) $t=0$ s; (b) $t=0.01$ s; (c) $t=0.02$ s; (d) $t=0.03$ s; (e) $t=3.01$ s; (f) $t=3.02$ s; (g) $t=3.03$ s; (h) $t=3.04$ s

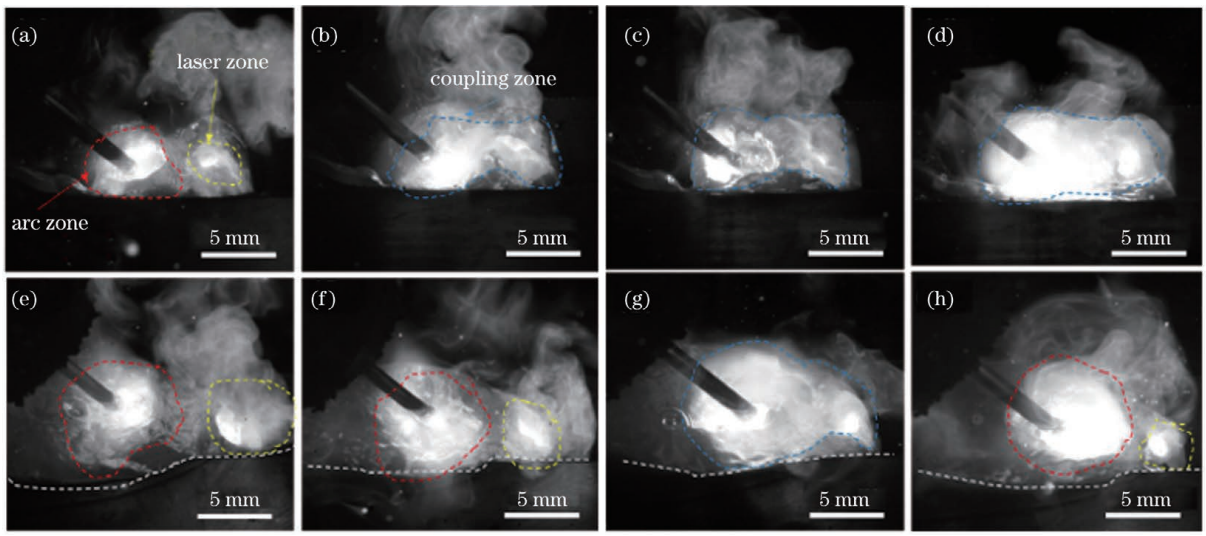

图 4 $d=4$ mm 时不同时刻激光和电弧等离子体形貌。(a)$t=0$ s;(b)$t=0.01$ s;(c)$t=0.02$ s;(d)$t=0.03$ s;(e)$t=3.01$ s;(f)$t=3.02$ s;(g)$t=3.03$ s;(h)$t=3.04$ s

Fig. 4 Profiles of laser and arc plasma at different moments with $d=4$ mm. (a) $t=0$ s; (b) $t=0.01$ s; (c) $t=0.02$ s; (d) $t=0.03$ s; (e) $t=3.01$ s; (f) $t=3.02$ s; (g) $t=3.03$ s; (h) $t=3.04$ s

等离子体的体积较大、亮度较弱,耦合不充分。随着热源继续移动,等离子体逐渐相互连接,等离子体亮度增加,耦合逐渐剧烈,如图 4(d)所示。图 4(e)、(f)所示为焊接稳定时的等离子体形貌。随着焊接过程的进行,熔池表面出现波动,激光小孔周围的等离子向焊接方向倾斜[图 4(e)],电弧和激光作用在不同平面上,导致电弧和激光出现不耦合现象[图 4(f)]。而后随着熔池进一步波动,熔池前部流体填满坡口,激光等离子体和电弧重新作用在同一平面内,电弧和激光等离子体重新连接,如图 4(g)所示。焊接热源继续移动,熔池表面再次波动,激光和电弧再次出现分离,如图 4(h)所示。与光丝间距为 2 mm 时相比,光丝间距为 4 mm 时电弧和激光等离子体连接过程中等离子体面积增大、亮度减弱,整个等离子体区域变长,因此其激光和电弧耦合效应没有光丝间距为 2 mm 时显著。

当光丝间距为 6 mm 时,起焊时激光和电弧距离较远,基本不耦合,如图 5(a)、(b)所示。随着焊接热源移动,电弧和激光等离子体开始连接[图 5(c)],随后又分开[图 5(d)],整个起焊过程等

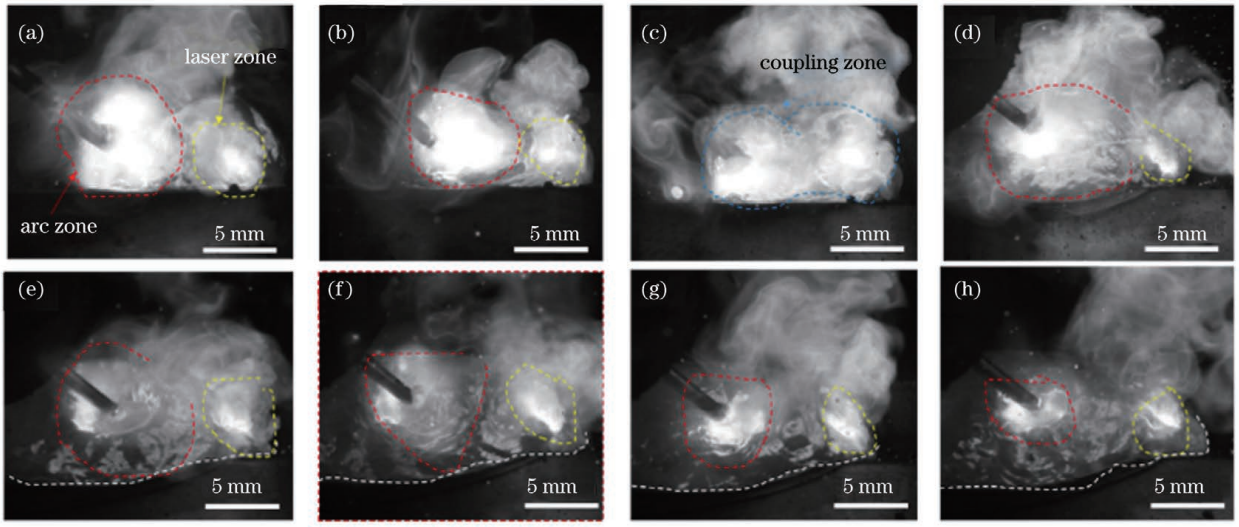

图 5　d=6 mm 时不同时刻激光和电弧等离子体形貌。(a)t=0 s;(b)t=0.01 s;(c)t=0.02 s;(d)t=0.03 s;(e)t=3.01 s;(f)t=3.02 s;(g)t=3.03 s;(h)t=3.04 s

Fig. 5　Profiles of laser and arc plasma at different moments with d=6 mm. (a) t=0 s; (b) t=0.01 s;(c) t=0.02 s; (d) t=0.03 s; (e) t=3.01 s; (f) t=3.02 s; (g) t=3.03 s; (h) t=3.04 s

离子体没有完全耦合。当焊接达到稳定状态时[图 5(e)、(f)],激光和电弧熔化液体形成共同熔池[图 5(e)],但由于激光和电弧的距离较远,不存在耦合现象,等离子体始终处于分离状态。

3.2　坡口中激光-电弧复合焊的熔池流动行为

图 6～8 分别展示了光丝间距为 2,4,6 mm 时高速摄像机拍摄的熔池形态。可以看到,当光丝间距为 2 mm 时,激光熔池和电弧熔池是共熔池,如图 6(a)所示。随着焊接热源移动,如图 6(b)所示,液态金属增多,逐渐填满坡口,熔池的最大宽度与坡口宽度一致。随着热源进一步移动,熔池出现波动,整个熔池表面不平整,导致激光小孔位置和形状发生变化,如图 6(c)所示。熔化的焊丝进一步增多,熔池宽度大于坡口宽度,整个熔池表面上移,坡口被填满,小孔到焊丝端部距离增大,如图 6(d)所示。图 6(e)～(h)所示分别为焊接稳定后熔池的表面形态和小孔表面形貌。焊接过程稳定后,焊丝末端和小孔表面的距离比起焊时明显增大,进一步证明了液面升高,实际光丝间距增大。此时小孔表面位于熔池前部,整个熔池形状为电弧区域较宽、激光作用

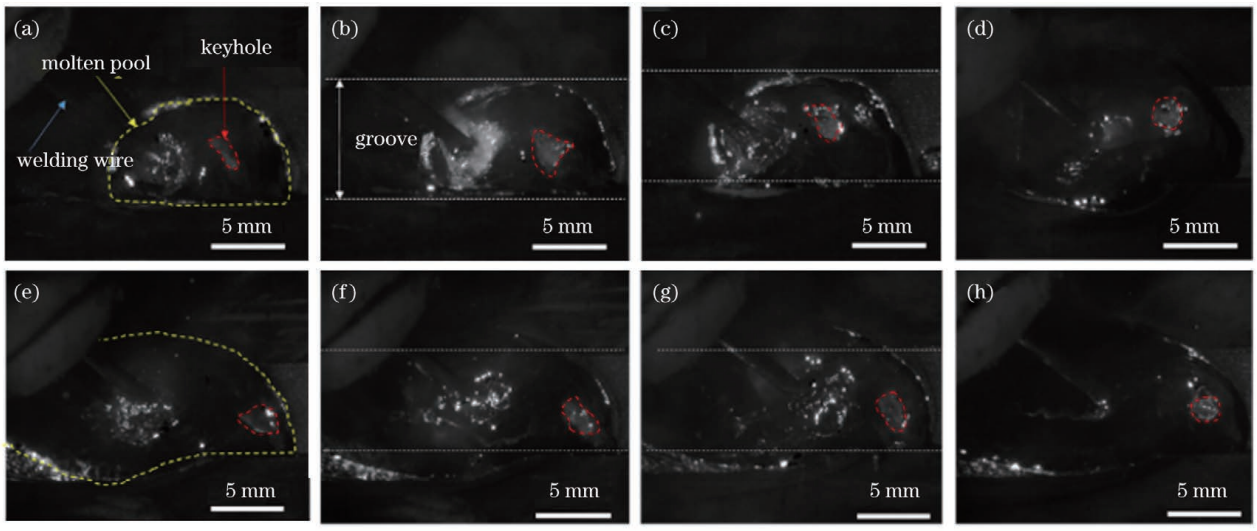

图 6　d=2 mm 时不同时刻复合焊熔池形态。(a)t=0 s;(b)t=0.1 s;(c)t=0.2 s;(d)t=0.3 s;(e)t=3.1 s;(f)t=3.2 s;(g)t=3.3 s;(h)t=3.4 s

Fig. 6　Dynamic characters of molten pool at different moments with d=2 mm. (a) t=0 s; (b) t=0.1 s; (c) t=0.2 s; (d) t=0.3 s; (e) t=3.1 s; (f) t=3.2 s; (g) t=3.3 s; (h) t=3.4 s

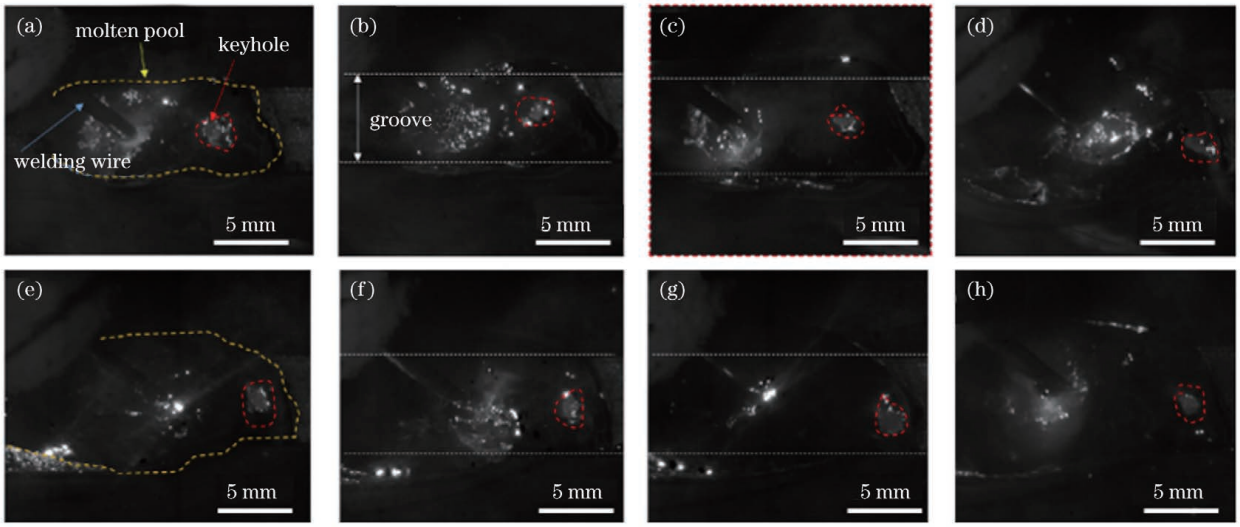

图 7 $d=4$ mm 时不同时刻复合焊熔池形态。(a)$t=0$ s;(b)$t=0.1$ s;(c)$t=0.2$ s;(d)$t=0.3$ s;(e)$t=3.1$ s;(f)$t=3.2$ s;(g)$t=3.3$ s;(h)$t=3.4$ s

Fig. 7 Dynamic characters of molten pool at different moments with $d=4$ mm. (a) $t=0$ s; (b) $t=0.1$ s; (c) $t=0.2$ s; (d) $t=0.3$ s; (e) $t=3.1$ s; (f) $t=3.2$ s; (g) $t=3.3$ s; (h) $t=3.4$ s

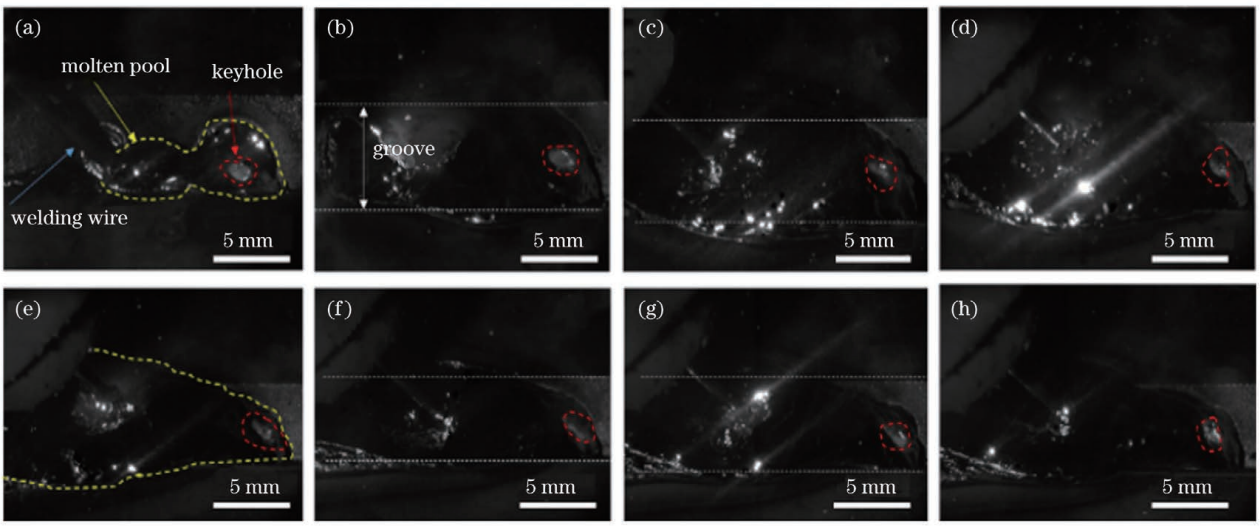

图 8 $d=6$ mm 时不同时刻复合焊熔池形态。(a)$t=0$ s;(b)$t=0.1$ s;(c)$t=0.2$ s;(d)$t=0.3$ s;(e)$t=3.1$ s;(f)$t=3.2$ s;(g)$t=3.3$ s;(h)$t=3.4$ s

Fig. 8 Dynamic characters of molten pool at different moments with $d=6$ mm. (a) $t=0$ s; (b) $t=0.1$ s; (c) $t=0.2$ s; (d) $t=0.3$ s; (e) $t=3.1$ s; (f) $t=3.2$ s; (g) $t=3.3$ s; (h) $t=3.4$ s

区域较窄[图 6(e)]。熔池表面波动剧烈,整个熔池表面形状发生变化[图 6(f)],导致激光入射面形状变化,进而影响小孔位置和小孔表面形状。因此,整个复合焊接过程中,在表面张力、电弧压力、电磁力以及小孔蒸气反作用力的共同作用下,熔化液体先在坡口中堆积,堆积到一定高度后,前部液体坍塌填充坡口,导致整个熔池液面起伏,进而影响激光入射面形状、小孔表面形貌及小孔位置,最终导致实际光丝间距变化,影响复合效果。

当光丝间距为 4 mm,起焊时激光熔池和电弧熔池直接连通,如图 7(a)所示。随着焊接热源移动,熔池前部液体逐渐填充坡口,小孔前部液体逐渐增多[图 7(b)],此时整个熔池宽度仍小于坡口宽度,熔融金属没有完全填满坡口[图 7(c)]。随着熔化金属逐渐增多,液体填满坡口,熔池宽度大于坡口宽度[图 7(d)]。图 7(e)、(f)所示为焊接稳定过程中熔池形貌。从图 7(e)可以看到,电弧区域的熔池较宽而激光作用区域的熔池较窄,进一步表明焊接电弧主要起到填充盖面作用,此时激光小孔作用位置在熔池前部,熔池前部液面明显低于坡口边缘

[图 7(g)]。与光丝间距为 2 mm 的情况相比，光丝间距为 4 mm 时整个焊接过程中熔池前部(激光作用区域)明显变窄，小孔位置前端液体变少，整个熔池面积增大。对比两种光丝间距下的等离子形态，发现光丝间距为 4 mm 时等离子体出现周期性耦合，主要是因为熔池液面波动导致光丝间距出现波动，进而出现耦合波动。尽管在 2 mm 光丝间距下激光和电弧能出现完全耦合，但由于光丝间距太小，下落的熔滴距离小孔位置处喷出的等离子体太近，容易出现飞溅，不利于焊缝成形。

图 8 所示为 6 mm 光丝间距时的熔池形态，可以看到，激光和电弧也是共熔池，如图 8(b)所示。随着焊接热源移动，激光小孔处熔池较窄且较浅，熔池宽度小于坡口边缘宽度，小孔明显位于坡口内部，而弧焊焊丝位于坡口上部表面。熔化的金属逐渐增多，液体填满坡口，但此时电弧区域的熔池较宽而激光作用区域的熔池较窄。激光小孔作用位置一直处于熔池最前端，始终与电弧区域的熔池不在同一水平面上，进而影响电弧和激光等离子体的耦合。此时激光作用区域的熔池相比光丝间距为 4 mm 时，变得更窄更长。

3.3 坡口中激光和电弧的等离子体耦合机制

根据所拍摄的电弧和激光等离子体形态，图 9 展示了光丝间距为4mm时激光和电弧在纵截面和

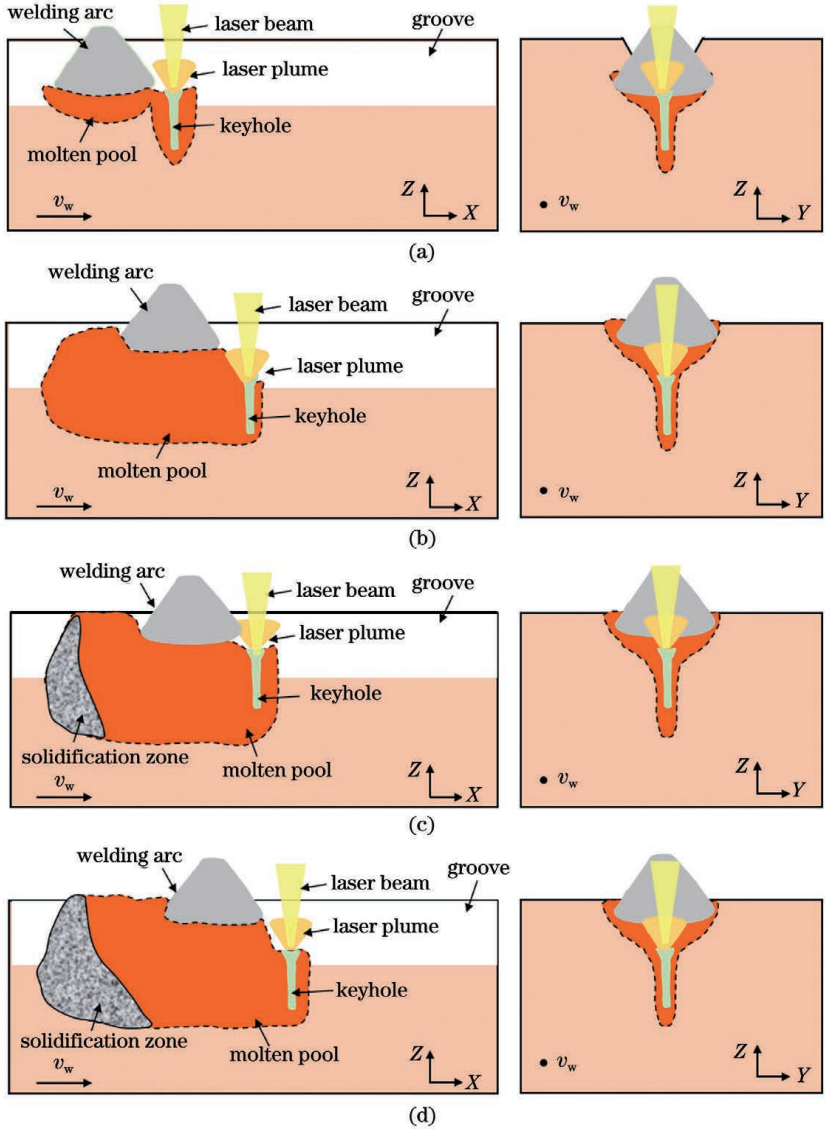

图 9 坡口中激光和电弧等离子体耦合机理示意图(d=4 mm)。(a)起焊时在坡口底部耦合；(b)电弧区域液面上升，耦合分离；(c)熔池液面波动再次耦合；(d)激光区-电弧区液面高度差导致耦合分离

Fig. 9 Coupling mechanism of laser and arc plasma at the groove with d=4 mm. (a) Coupling at the bottom of groove at the beginning of welding; (b) coupling separation due to the increase of liquid level in arc zone; (c) coupling due to molten pool level fluctuation; (d) coupling separation due to liquid level difference between laser zone and arc zone

横截面上的耦合过程。图 9(a)所示为起焊时，激光与电弧形成共同熔池，熔池中液体发生堆积，激光和电弧等离子体处在同一高度，位于同一水平面内，但等离子体只有部分重叠，两者为弱耦合，熔池波动不剧烈。随着焊接热源移动，熔池前部液体填充坡口底部[图 9(b)]，激光作用区域的熔池表面下移，使得激光直接照射的表面下移，但熔池后部的电弧区域液面仍然较高，最终导致电弧和激光不在同一水平面上，激光和电弧耦合不充分，复合效果变差，但此时焊缝表面成形由电弧决定，与单独弧焊时表面成形一致，有利于焊缝成形。随后，随着热源移动和熔池液面波动，激光作用区域液面升高，与电弧区域的液面又在同一水平面上[图 9(c)]，两者再次耦合。随后热源移动，激光作用区域液体再次填充坡口，液面下降，激光和电弧等离子体分离，耦合分离[图 9(d)]。因此，在坡口中进行激光复合焊接时，随着熔池波动，熔池内液体进行坡口填充，电弧和激光耦合效果也随之改变，这一点与激光和电弧平板焊接时明显不同。

由此可见，激光和电弧在坡口进行复合焊接时，激光和电弧的耦合主要由熔池液面状态决定。熔池液面在表面张力、重力等作用下，起初在坡口内堆积，随后液面开始铺展，整个堆积-铺展过程中焊丝端部和激光小孔之间的距离发生变化，进而影响电弧和激光等离子体的耦合效果。因此，当光丝间距为 4 mm 左右时，电弧熔化焊丝速率较慢(电流较小)或焊接速度较快时，后部焊丝熔化的液体来不及向激光小孔方向流淌，使得激光和电弧始终不在同一水平面上，不能获得较好的耦合效果。当焊丝熔化速率较快(电流较大)或焊接速度较慢时，激光和电弧周期性耦合频率增大。另外，坡口底部形状也会影响熔池液面波动。坡口底部越宽，若焊丝熔化液体一定，液面堆积高度较小，熔池前、后液面的高度差就越小，越有利于激光和电弧的耦合。

3.4　坡口中激光-电弧复合焊的焊缝成形特征

图 10 分别显示了在坡口中激光-电弧复合焊的光丝间距为 2，4，6 mm 时焊缝的横截面成形及表面成形特征。可以看到：当光丝间距为 2 mm 时，由于电弧和激光处于完全耦合状态，焊缝熔深较大(约 12.2 mm)，但焊缝表面出现飞溅，成形较差；当光丝间距为 4 mm 时，熔深略有降低(约 10.2 mm)，但焊缝表面成形较好，焊缝光滑且连续；当光丝间距为 6 mm 时，焊缝表面成形较好，但熔深仅为 8.8 mm 左右，这说明在 V 型坡口中光丝间距超过 6 mm 时耦合效果不明显。进一步说明在本研究的坡口中进行激光-电弧复合焊时，最佳耦合光丝间距为 4 mm 左右，相比已报道的在平板上激光-电弧复合焊耦合距离有所降低[16]。

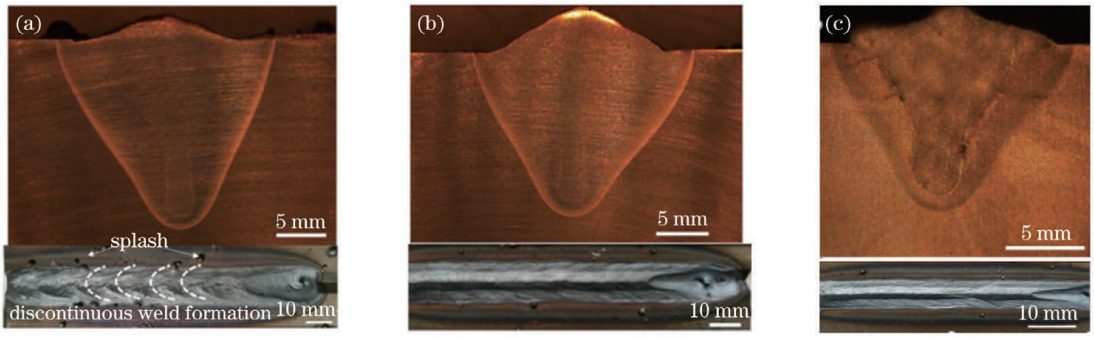

图 10　不同光丝间距(d)时焊缝横截面及表面成形特征(激光功率 P=7 kW，电弧电流 I=240 A，焊接速度 v=0.5 m/min)。(a)d=2 mm；(b)d=4 mm；(c)d=6 mm

Fig. 10　Profiles of welding surface and cross section under different arc tip and laser distances (P=7 kW, I=240 A, and v=0.5 m/min). (a) d=2 mm; (b) d=4 mm; (c) d=6 mm

4　结　　论

在坡口中进行激光-电弧复合焊接时，采用激光引导的方式，光丝间距为 2 mm 时，电弧和激光等离子体出现强烈耦合，电弧和激光等离子体从起焊到焊接过程稳定均连接在一起，等离子体亮度较高，飞溅增多，激光和电弧共熔池，熔池波动剧烈，熔池较浅且较宽，所获得的焊缝熔深较大，焊缝表面成形较差。当光丝间距为 4 mm 时，激光和电弧等离子体处于周期性耦合状态。随着电弧底部坡口填充高度增加，激光和电弧不在同一水平面内，光丝间距增大，电弧和激光等离子体分离；当电弧底部液体堆积到一定高度后，在重力和表面张力的作用下液体向激光作用区域流淌，液面趋于水平，光丝间距减小，

激光和电弧开始耦合，熔池连接在一起；焊缝表面成形较好，焊缝深度略有降低。当光丝间距超过 6 mm 时，激光和电弧在坡口中无耦合现象。因此，在坡口中进行激光-电弧复合焊时，由于存在熔池流体堆积现象，整个熔池液面处于倾斜状态，激光和电弧的最佳耦合光丝间距较小，为 4 mm 左右，焊缝熔深较大且表面成形较好。

参 考 文 献

[1] Viano D M, Ahmed N U, Schumann G O. Influence of heat input and travel speed on microstructure and mechanical properties of double tandem submerged arc high strength low alloy steel weldments[J]. Science and Technology of Welding and Joining, 2000, 5(1): 26-34.

[2] Amodeo C M, Lai W J, Lee J, et al. Failure modes of gas metal arc welds in lap-shear specimens of high strength low alloy (HSLA) steel[J]. Engineering Fracture Mechanics, 2014, 131: 74-99.

[3] Zou Z D, Li Y J, Yin S K. Toughness and TEM analysis of simulated CGHAZ of HQ130 steel[J]. Transactions of the China Welding Institution, 1998, 19(3): 141-146.
邹增大, 李亚江, 尹士科. HQ130 钢焊接 CGHAZ 韧性及 TEM 分析[J]. 焊接学报, 1998, 19(3): 141-146.

[4] Si Z H. Processing research of MAG welding for WELDOX960 high-tensile steel[J]. Aerospace Manufacturing Technology, 2012(2): 21-24.
司子华. WELDOX960 高强钢 MAG 焊的工艺研究[J]. 航天制造技术, 2012(2): 21-24.

[5] Lan L Y, Kong X W, Qiu C L, et al. Influence of microstructural aspects on impact toughness of multi-pass submerged arc welded HSLA steel joints[J]. Materials & Design, 2016, 90: 488-498.

[6] Pamnani R, Jayakumar T, Vasudevan M, et al. Investigations on the impact toughness of HSLA steel arc welded joints[J]. Journal of Manufacturing Processes, 2016, 21: 75-86.

[7] Xu B, Ma C Y, Li L, et al. Effect of heat input on microstructure and property of weld joints of a 1200 MPa grade HSLA steel[J]. Chinese Journal of Materials Research, 2017, 31(2): 129-135.
徐彬, 马成勇, 李莉, 等. 热输入对 1200 MPa 级 HSLA 钢焊缝组织性能的影响[J]. 材料研究学报, 2017, 31(2): 129-135.

[8] Anant R, Ghosh P K. Ultra-narrow gap welding of thick section of austenitic stainless steel to HSLA steel[J]. Journal of Materials Processing Technology, 2017, 239: 210-221.

[9] Cai X Y, Fan C L, Lin S B, et al. Molten pool behaviors and weld forming characteristics of all-position tandem narrow gap GMAW[J]. The International Journal of Advanced Manufacturing Technology, 2016, 87(5/6/7/8): 2437-2444.

[10] Cai X Y, Lin S B, Fan C L, et al. Molten pool behavior and weld forming mechanism of tandem narrow gap vertical GMAW[J]. Science and Technology of Welding and Joining, 2016, 21(2): 124-130.

[11] Sokolov M, Salminen A, Kuznetsov M, et al. Laser welding and weld hardness analysis of thick section S355 structural steel[J]. Materials & Design, 2011, 32(10): 5127-5131.

[12] Zhan X, Zhang D, Wei Y, et al. Research on the microstructure and properties of laser-MIG hybrid welded Joint of Invar alloy[J]. Optics & Laser Technology, 2017, 97: 124-136.

[13] Chen C, Wang W Y, Li D Y, et al. Effect of beam oscillation on microstructure and properties of laser-TIG hybrid welding of D406A ultra-high strength steel[J]. Journal of Manufacturing Processes, 2020, 57: 798-805.

[14] Silva R G N, Paço C M M, Rodrigues M B, et al. A comparison between LBW and hybrid laser-GMAW processes based on microstructure and weld geometry for hardenable steels[J]. The International Journal of Advanced Manufacturing Technology, 2020, 110(9/10): 2801-2814.

[15] Gao M, Zeng X Y, Yan J, et al. Microstructure characteristics of laser-MIG hybrid welded mild steel[J]. Applied Surface Science, 2008, 254(18): 5715-5721.

[16] Hu L H, Huang J, Liu C T, et al. Effects of coupling between the laser plasma and two arcs on metal transfer in CO_2 laser double-wire MIG hybrid welding[J]. Optics & Laser Technology, 2018, 105: 152-161.

[17] Ren W J, Zheng H J, Li Z G, et al. Effects of pulse arc on droplet transfer and spatter of laser pulsed-arc hybrid welding[J]. Chinese Journal of Lasers, 2020, 47(4): 0402007.
任闻杰, 郑惠锦, 李铸国, 等. 脉冲电弧对激光脉冲电弧复合焊熔滴过渡与飞溅的影响[J]. 中国激光, 2020, 47(4): 0402007.

[18] Zhang W, Tang B, Guo Y B, et al. Investigation on surface forming and stability of laser + pulse melting gas metal arc hybrid welding[J]. Laser & Optoelectronics Progress, 2020, 57(17): 171401.
张旺, 唐彬, 郭彦兵, 等. 激光+脉冲熔化极气体保护复合焊接表面成形及稳定性研究[J]. 激光与光电

子学进展, 2020, 57(17): 171401.

[19] Chen Z W, Ma C Y, Chen B, et al. Microstructure and properties of medium-thick stainless steel by laser-MIG hybrid welding[J]. Laser & Optoelectronics Progress, 2020, 57(23): 231405.
陈志伟, 马程远, 陈波, 等. 激光-MIG 复合焊接中厚度不锈钢组织及性能研究[J]. 激光与光电子学进展, 2020, 57(23): 231405.

[20] Cao X, Wanjara P, Huang J, et al. Hybrid fiber laser-arc welding of thick section high strength low alloy steel[J]. Materials & Design, 2011, 32(6): 3399-3413.

[21] Li H Y, Tan C W, Zhang Q, et al. Effect of heat source order on coupling mechanism and mechanical properties of joints in laser-arc hybrid welding of HG785D high-strength steels[J]. Chinese Journal of Lasers, 2018, 45(5): 0502006.
李昊岳, 檀财旺, 张强, 等. 热源顺序对 HG785D 高强钢激光-电弧复合焊耦合机理与接头性能的影响[J]. 中国激光, 2018, 45(5): 0502006.

Plasma Coupling Behavior of Laser-Arc Hybrid Welding in Groove

Zhou Jian, Shao Chendong, Cui Haichao*, Tang Xinhua, Lu Fenggui

School of Materials Science and Engineering, Shanghai Jiao Tong University, Shanghai 200240, China

Abstract

Objective BG890QL low-alloy high-strength steel is widely used in the field of construction machinery because of its high strength and low-temperature toughness. The conventional arc welding method, on the other hand, results in a low welding efficiency of medium thickness plate BG890QL. Many scholars use the laser hybrid welding method to study the medium thickness plate welding to improve the welding efficiency of medium thickness plate BG890QL low alloy high strength steel. A large body of literatures have been written about laser hybrid welding on flat plates, and many research have been conducted on the arc and laser coupling mechanism, droplet transfer morphology, weld formation, and weld performance in the welding process. However, to increase the penetration of laser-arc hybrid welding, the upper part is generally grooved, and the welding depth is increased by laser while the arc covers the surface to fill, which can ensure the weld depth and weld formation, resulting in laser-arc hybrid welding being widely used in the field of medium thickness plate welding. When the laser-arc hybrid welding is carried out in the groove, with the fluctuation of the molten pool, the liquid in the molten pool fills the groove, resulting in that the arc and laser are not in the same horizontal plane, and the coupling effect of laser and arc plasma also changes, which is different from that of laser and arc plate welding. It is necessary to study the coupling mechanism of laser and arc plasma in the groove.

Methods Laser-arc hybrid welding was performed on 16-mm thick BG890QL low-alloy high-strength steel with V-groove (the groove angle was 50° and the depth of groove bottom is 8 mm). The laser-arc hybrid welding parameters were as follows: laser power is 7 kW, arc welding current is 240 A, welding voltage is 22 V, and welding speed is 0.5 m/min. High-speed camera was used to capture the morphology of arc and laser-plasma, as well as the flow behavior of a molten pool. The optical microscope Zeiss-AxioCam MRc5 was used to examine the microstructure.

Results and Discussions According to the morphology of arc and laser-plasma and the flow behavior of the molten pool (as shown in Figs. 3–8), the coupling mechanism of laser and arc in the groove with the laser-arc distance of 4 mm is obtained, as shown in Fig. 9. The figure shows a longitudinal section on the left and a cross-section on the right. Fig. 9 (a) depicts when the laser and arc begin welding, they form a common molten pool in which liquid accumulates. The laser and the arc plasma are both at the same height and in the same horizontal plane, but the plasma only partially overlaps. The two are in the weak coupling, and the molten pool fluctuation is not severe. As the welding heat source moves, the liquid in the front of the weld pool fills the bottom of the groove [as shown in Fig. 9 (b)], the surface of the weld pool remains in the laser action area, and the liquid level in the arc area at the back of the weld pool remains high, resulting in that the arc and the laser are not in the same horizontal plane, the coupling between the laser and the arc is insufficient, and the composite effect becomes worse. It is the same as single arc welding, which is advantageous for weld forming. Then, as the heat source moves and the molten pool

liquid level fluctuates, the liquid level in the laser action area rises, and the arc is in the same horizontal plane [as shown in Fig. 9 (c)]. The two are coupled again. The heat source then moves, the liquid in the laser area refills the groove, the liquid level drops, the laser and arc plasma is separated, and the coupling is separated [as illustrated in Fig. 9 (d)].

Conclusions Laser-arc hybrid welding is carried out in the groove, when the laser-arc distance is 2 mm, the arc and laser-plasma are strongly coupled. From the beginning of the welding process to the end of the welding process, the arc and laser-plasma are inextricably linked. The plasma brightness is high, the spatter is increasing, and the weld pool is violently fluctuating; the results show that weld penetration is high but weld surface forming is poor. The laser and arc plasma are periodically coupled when the laser-arc distance is 4 mm. With the increase of the filling height at the bottom of the groove, the laser and the arc are not in the same horizontal plane, the distance between the laser and arc increases, and the arc and laser-plasma are separated; When the liquid at the bottom accumulates to a certain height, it flows to the laser action area due to gravity and surface tension; the liquid level tends to be horizontal, and the laser-arc distance decreases; the laser and the arc begin to couple, and the molten pool is joined together; the weld surface is well-formed, and the weld depth is slightly reduced. When the laser-arc distance exceeds 6 mm, there is no coupling between the laser and the arc in the groove. During laser-arc hybrid welding in the groove, the liquid level of the whole weld pool is inclined due to the accumulation of liquid in the weld pool. The range of the best coupling distance of laser and arc is narrow (~4 mm), and the weld penetration is high and the surface forming is good.

Key words laser technique; laser-arc hybrid welding; low-alloy high-strength steel; groove; coupling mechanism